Colorless Bi2O3-containing borophosphate glasses with high refractivity

K. Hayashi, Grégory Tricot, A. Saitoh

Journal of the Ceramic Society of Japan 131 [12] 889-893 2023
DOI https://doi.org/10.2109/jcersj2.23138

JCS-Japan

FULL PAPER

Colorless Bi_2O_3-containing borophosphate glasses with high refractivity

Katsuki Hayashi[1], Grégory Tricot[2] and Akira Saitoh[1,†]

[1]Graduate School of Science and Engineering, Ehime University, Matsuyama, Ehime 790–8577, Japan
[2]Laboratoire de Spectroscopie pour les Interactions, la Réactivité & l'Environnement (LASIRE)–UMR CNRS 8516, Université de Lille, F-59000 Lille, France

The effects of P_2O_5 substitution on the coordination structure of a Bi^{3+} in Bi_2O_3–B_2O_3 glasses were examined by applying ^{11}B and ^{31}P MAS-NMR spectroscopy. Observation of the wide optical bandgap after the substitution revealed a substantial difference in the solvation shell structure between the P_2O_5 substituted and the P_2O_5-free Bi_2O_3-containing glasses, i.e., the P_2O_5 substitution replaced by the B_2O_3 is effective for forming the solvation shell, which leads to weak ligand field around a Bi^{3+}. We report the optical properties of the Bi_2O_3–P_2O_5–B_2O_3 glass providing a wide optical bandgap (∼3.6 eV) and high refractive index (∼2.0).

Key-words : Borophosphate glass, Refractive index, Nuclear magnetic resonance, Structure

[Received August 18, 2023; Accepted September 22, 2023]

1. Introduction

Bi_2O_3-containing oxide glasses are widely employed in applications for optical devices.[1)] Although Bi_2O_3–B_2O_3 glasses that have many excellent physical properties are a highly desired host for optically active ions,[2)–4)] their fatal drawback is coloration.[5),6)] This issue, ascribed to a strong ligand field around a cation, was resolved by a co-doping technique.[7),8)] For instance, Saitoh et al. demonstrated the "solvation shell" model based on directly observing the ligand structures of Ce^{3+} and Er^{3+} in SiO_2 glasses to understand the striking doping effects of P_2O_5. The concept of solvation shell of ions in the SiO_2 glass, i.e., preferential coordination of doped P_2O_5 around the rare-earth ions, is favorable for designing highly efficient luminescence as an optical material. As a result, the photoluminescence properties of Ce^{3+} and Er^{3+} in those samples showed a slight Stokes shift and high emission intensity. Hence, we can consider the substitution of B_2O_3 by P_2O_5 in the Bi_2O_3–B_2O_3 glasses as effective in realizing colorless property, keeping a high refractive index, which will weaken the ligand field of a Bi^{3+}.

Little qualitative structure by the effect of P_2O_5 has been reported in the binary Bi_2O_3–P_2O_5 glasses because of the narrow glass formation region up to 40 mol % of Bi_2O_3.[5),9),10)] It is considered that the borophosphate glasses consisting of tetrahedrally coordinated PO_4–BO_4–PO_4 linkage can widen the glass formation region[4),11)] and thus offer the possibility of providing high refractive index materials.

The purpose of this study is to present Bi_2O_3–P_2O_5–B_2O_3 glasses with high concentrations of Bi_2O_3, wide optical bandgap, and high refractive index. In addition, the glass network was characterized by ^{11}B and ^{31}P MAS-NMR spectroscopies to determine the substitution effect of P_2O_5 on the coordination structure around a Bi^{3+}.

2. Experimental

Glass samples were prepared using the conventional melt-quenching method. Reagent grades of Bi_2O_3 (99.99 %), B_2O_3 (99.9 %), and $BiPO_4$ (99.9 %) were used as raw materials. The nominal molar composition is xBi_2O_3–yP_2O_5–$(100-x-y)B_2O_3$ with $40 \leq x \leq 60$, $0 \leq y \leq 20$. Batches that yielded 12–15 g were mixed and then melted for 30 min at 1000 °C in an alumina crucible in an electric furnace in the air. The dissolution of Al_2O_3 into the sample was 1–2 mol % by SEM-EDS. The melts were poured into a preheated stainless-steel mold and then annealed to remove residual thermal stress in the air for 24 h at 360–470 °C, depending on glass transition temperatures. The amorphous nature of the resulting bulk glasses was confirmed by X-ray diffraction analysis.

The density of the bulk sample was determined using the Archimedes method with kerosene as an immersion liquid for the glasses at room temperature. The estimated uncertainties due to composition fluctuations were ±0.01 g/cm^3.

The refractive index was measured using the refractometer for a $3 \times 3 \times 10$ mm^3 rectangular glass rod at 587.6 nm wavelengths. The estimated uncertainties due to composition fluctuations were ±0.01. Optical transmission spectra were measured using a 1 mm-thick plate and a ∼2 μm thick film. The film was obtained from a piece of glass balloon blown from each glass melt using an alumina pipe.

† Corresponding author: A. Saitoh; E-mail: asaito@ehime-u.ac.jp

The ^{11}B and ^{31}P MAS-NMR experiments were performed at 256.7 and 323.9 MHz on an 18.8 T spectrometer (AVANCE III, Bruker) using a 3.2-mm probe head operating at a spinning frequency of 20 kHz. The ^{11}B MAS-NMR spectra were obtained with a $\pi/10$ flip angle of 1.0 µs, recycle delay (rd) of 5 s, and 1024 transients. The ^{31}P MAS-NMR spectra were obtained with a $\pi/6$ flip angle of 1.8 µs, rd of 120 s, and 32 transients. The ^{11}B and ^{31}P chemical shifts are respective to $NaBH_4$ and H_3PO_4 as −42.06 and 0 ppm, respectively. The NMR spectra were decomposed using the dmfit software[12] to extract the chemical shift and relative proportions parameters.

3. Results and discussion

Figures 1(a) and 1(b) show the compositional dependences of the density and refractive index measured at 587.6 nm of wavelength in the xBi_2O_3–yP_2O_5–$(100-x-y)$-B_2O_3 glasses. In each Bi_2O_3 concentration sample, the density and refractive index decrease with increasing P_2O_5, which replaces B_2O_3. Note that the $x = 60$, $y = 10$ sample particularly presents a high refractive index (~2.1) measured at 587.6 nm and a small photoelastic constant ($+0.5 \times 10^{-12}$ Pa^{-1}) measured at 632.8 nm.

Figures 2(a)–2(c) show the compositional dependences of optical transmission spectra of the xBi_2O_3–yP_2O_5–$(100-x-y)B_2O_3$ glasses. The optical absorption edges of the Bi_2O_3–P_2O_5–B_2O_3 glasses blueshift, substituting B_2O_3 with P_2O_5. While the optical absorption edges of the Bi_2O_3–P_2O_5–B_2O_3 glasses redshift with increasing Bi_2O_3 concentration. The samples of large concentrations of Bi_2O_3 (x) and small amount of P_2O_5 (y) are likely to show pale yellow. Figure 2(d) compares the transmission spectra of the bulk and thin film samples. Notably, the $x = 50$, $y = 20$ sample presents the absorption edge being near a deep ultraviolet region (<350 nm).[13]

Figures 3(a) and 3(b) show the compositional dependences of the absorption coefficient spectra and Tauc plots determined from the absorption coefficients of the $50Bi_2O_3$–$50B_2O_3$ ($x = 50$, $y = 0$) and the $50Bi_2O_3$–$20P_2O_5$–$30B_2O_3$ ($x = 50$, $y = 20$) glasses. Note that the optical bandgaps are determined from the Tauc plot $(\alpha h\nu)^{1/2}$ versus photon energy $h\nu$, where α denotes the optical absorption coefficient. Here, the photon energy dependence of the optical absorption of glass can be expressed as $(h\nu - E)^2/h\nu$, where E denotes the optical band gap.[14] The optical bandgap of the $50Bi_2O_3$–$20P_2O_5$–$30B_2O_3$ glass increases by ~0.2 eV with the incorporation of P_2O_5.

Figures 4(a)–4(c) show ^{11}B MAS-NMR spectra, including the proportions of three- and four-coordinated borate units of the xBi_2O_3–yP_2O_5–$(100-x-y)B_2O_3$

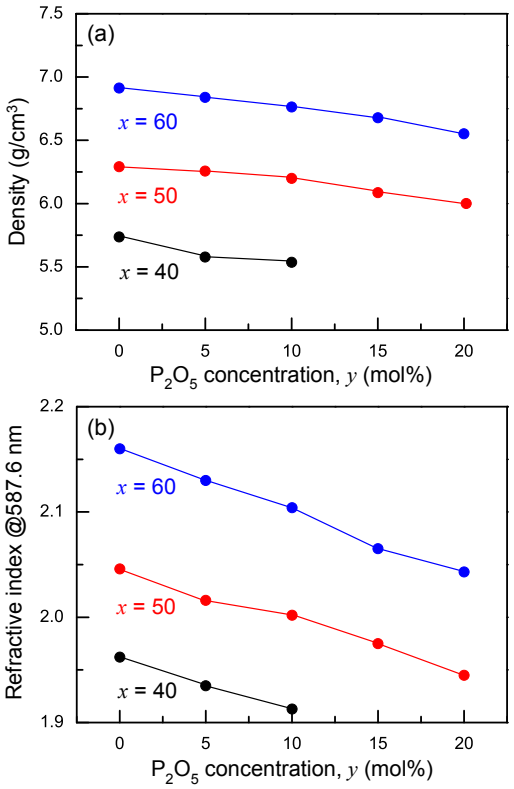

Fig. 1. Compositional dependences of the (a) density and (b) refractive index of the xBi_2O_3–yP_2O_5–$(100-x-y)B_2O_3$ ($40 \le x \le 60$, $0 \le y \le 20$) glasses.

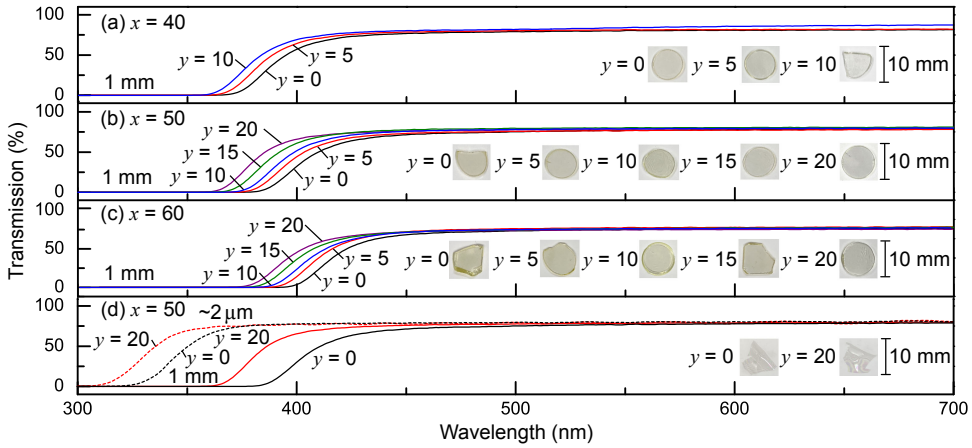

Fig. 2. Compositional dependences of optical transmission spectra of the xBi_2O_3–yP_2O_5–$(100-x-y)B_2O_3$ ($40 \le x \le 60$, $0 \le y \le 20$) glasses in the wavelength range 300–700 nm for samples with 1 mm and ~2 µm thicknesses. The dashed lines in (d) present the spectra for the film samples of $x = 50$, $y = 0$, 20.

glasses. Altogether, five different species can be observed with four B^{IV} and one B^{III} units. The assignments of each borate unit[4),15)] are listed in **Table 1**, and are derived from a 1D/2D NMR protocol applied to a similar system (SnO–B_2O_3–P_2O_5) in a previous study.[4)] As the concentrations of Bi_2O_3 (x) and substituted P_2O_5 (y) increase, the apparent ratio of B^{III} appears to increase. However, there is no clear regularity in the ratio of B^{III} to B^{IV}, and the ratio tends to increase within the error of the deconvolution of ^{11}B NMR spectrum. On the other hand, the proportions of each unit of $B^{IV}{}_{(1)}$–$B^{IV}{}_{(4)}$ do not essentially depend on the changes in Bi_2O_3 and P_2O_5 concentrations. However, the $x = 50$ and $y = 20$ sample shows a large proportion of B^{IV}; among them, the proportion of $B^{IV}{}_{(2)}$ and $B^{IV}{}_{(3)}$ is substantial. The experiments show that our glasses mainly contain three coordinated boron species (>65 %). The low proportion of $B^{IV}{}_{(1)}$ (<5 %) indicates a strong B^{IV}/B^{III} mixing. Moreover, the four-coordinated B is also adjacent to a Bi^{3+} as revealed by the significant presence of $B^{IV}{}_{(3)}$ unit.

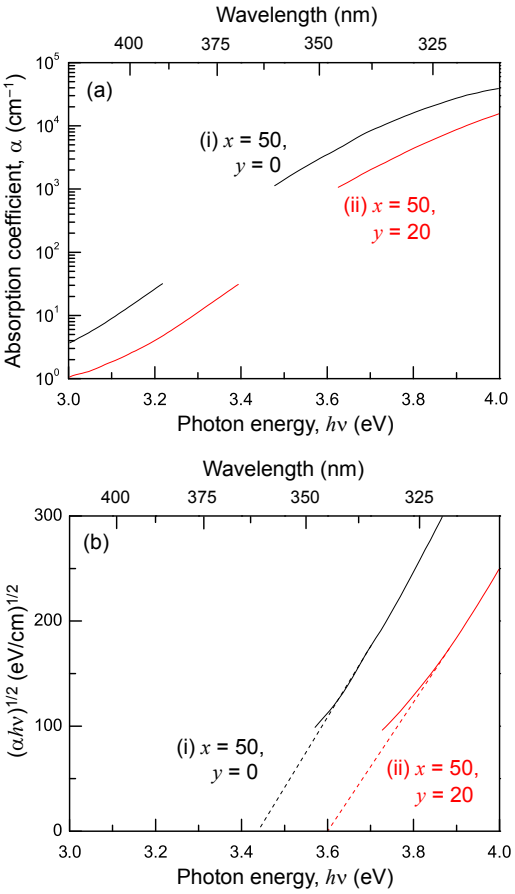

Fig. 3. (a) Absorption coefficient spectra and (b) Tauc plots of the $50Bi_2O_3$–$50B_2O_3$ and $50Bi_2O_3$–$20P_2O_5$–$30B_2O_3$ glasses with 1 mm and ~2 µm thickness. In (b), the dashed lines present the estimated optical bandgap of the $x = 50$, $y = 0$ and $x = 50$, $y = 20$ samples.

Figures 5(a)–5(c) show the ^{31}P MAS-NMR spectra with the proportions of phosphate units in the xBi_2O_3–yP_2O_5–$(100 - x - y)B_2O_3$ glasses. Three species around −18, −10, and 3 ppm can be observed with various proportions depending on the glass composition. The assignments of these three species are reported in Table 1 and are derived from the 1D/2D NMR protocol applied to the tin borophosphate glass containing a high amount of SnO.[4)] As the concentration of Bi_2O_3 (x) increases, the proportion of Q^1 decreases. On the other hand, as the concentration of P_2O_5 (y) increases, Q^0 and $Q^0{}_B$ decrease, and Q^1 increases. The $x = 50$ and $y = 20$ sample shows that $Q^0{}_B$ and Q^1 units are major species of the phosphate units.

According to the ^{31}P NMR spectra, the four-coordinated P is bound to the three- and four-coordinated B from the assignment of $Q^0{}_B$. The four coordinated P is terminated to a Bi^{3+} as a Q^1 or Q^0 unit. Hence, the coordination of the Bi^{3+} in the $50Bi_2O_3$–$20P_2O_5$–$30B_2O_3$ glass consists of PO_4 or BO_4 units. When the amount of P_2O_5 substitution is large, PO_4 is the primary ligand, which can be similar to the solvation shell structure by P_2O_5.[7),8)]

Figure 6 illustrates the coordination structure model of the borate and phosphate units in the vicinity of a Bi^{3+} in the $50Bi_2O_3$–$20P_2O_5$–$30B_2O_3$ ($x = 50$, $y = 20$) glass, which has an optical bandgap of 3.6 eV and a refractive index of 2.0. A possibility of the formal charges on the non-bridging oxygens (NBOs) belonging to the phosphate units is −1/2 of the Q^1 and Q^0 units. Because in a middle phosphate group, an electron is delocalized over two NBOs via pπ-dπ bonding. In other words, in the phosphate units, the formal charge on the NBO in the P–O bond is −0.5 due to the delocalization of electrons over the two NBOs via the Opπ–P3dπ bond.[7),16),17)] Then, ligands around a Bi^{3+} belong to this type of oxygens with the formal negative charge of −0.5, which is an intermediate value between conventional NBO (−1) and bridging oxygen (0). Therefore, the ligand field is considered weaker because the Bi^{3+} surroundings are not composed of large formal charged oxygens (−1). On the other hand, in the

Table 1. Assignments of each borate and phosphate unit were analyzed by the ^{11}B and ^{31}P MAS-NMR spectra of the xBi_2O_3–yP_2O_5–$(100 - x - y)B_2O_3$ glasses

Units and notation		Assignments	Refs.
Borate	$B^{IV}{}_{(1)}$	Connected to tetrahedral species $[B(OX^{IV})_4$ with X = P or B]	4, 15
	$B^{IV}{}_{(2)}$	Connected to at least one B^{III} units $[B(OX^{IV})_m(OB^{III})_k$ $(0 \le m \le 3, 1 \le k \le 4)]$	
	$B^{IV}{}_{(3)}$	Direct coordination to at least one Bi^{3+}	
	$B^{IV}{}_{(4)}$	Not assigned	
Phosphate	Q^1	Pyrophosphate unit with three non-bridging oxygen ions per phosphorus and one connected P atom	4
	$Q^0{}_B$	PO_4 tetrahedral unit with one bridging oxygen with to B^{III} or $B^{IV}{}_{(1)}$ and no connected P atom	
	Q^0	Orthophosphate unit with four non-bridging oxygen ions per phosphorus	

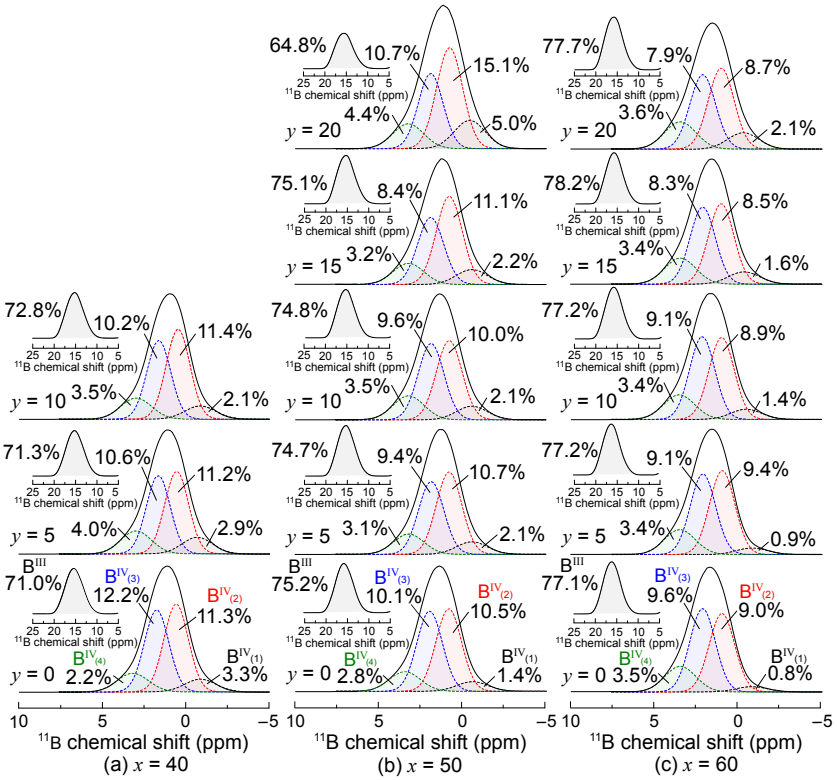

Fig. 4. ^{11}B MAS-NMR spectra of the xBi_2O_3–yP_2O_5–$(100 - x - y)B_2O_3$ glasses with (a) $x = 40$, $y = 0$, 5, and 10, (b) $x = 50$, $y = 0$, 5, 10, 15, and 20, and (c) $x = 60$, $y = 0$, 5, 10, 15, and 20. The B^{III} and B^{IV} ($B^{IV}_{(1)}$–$B^{IV}_{(4)}$) proportions are denoted, respectively. The notations (B^{III} and $B^{IV}_{(1)}$–$B^{IV}_{(4)}$) indicate the coordination number of oxygens in superscript and type in parenthesis.

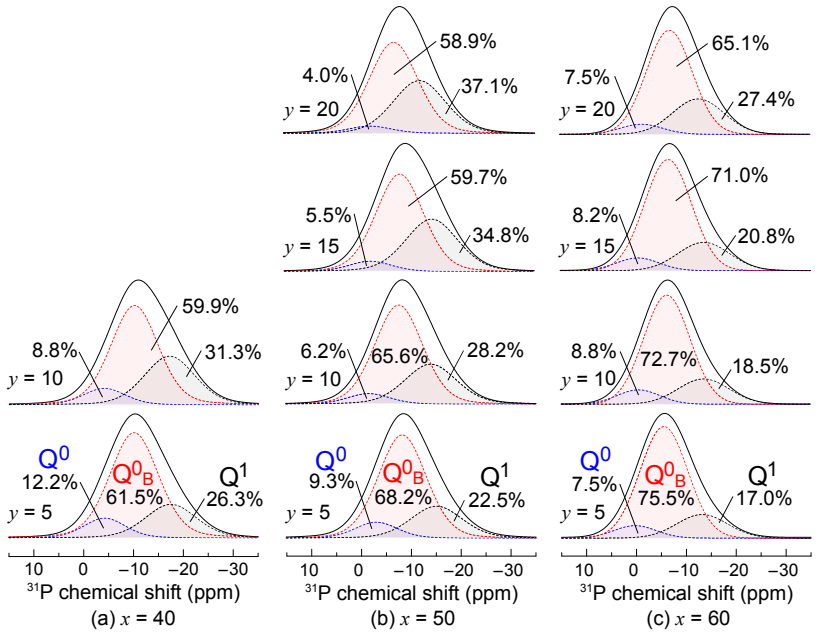

Fig. 5. ^{31}P MAS-NMR spectra of the xBi_2O_3–yP_2O_5–$(100 - x - y)B_2O_3$ glasses with (a) $x = 40$, $y = 5$ and 10, (b) $x = 50$, $y = 5$, 10, 15, and 20, and (c) $x = 60$, $y = 5$, 10, 15, and 20. The Q^0, Q^0_B, and Q^1 proportions are denoted, respectively. The notations (Q^0, Q^0_B, and Q^1) indicate the number of non-bridging oxygens in superscript.

BO_3 and BO_4 units, the charge of -1 is allocated to each oxygen if it is a three-coordinated oxygen, and the charge of $-3/4$ if it is a four-coordinated oxygen to compensate for the $+3$ charge of B. If BO_4 units were involved in the coordination in part, they would contribute to forming a weak ligand field since the net charge would be $-3/4$.[18] The fact that the coordination structure around a Bi^{3+} in the $40Bi_2O_3$–$60P_2O_5$ glass resembles a $BiPO_4$ crystal[5),19)]

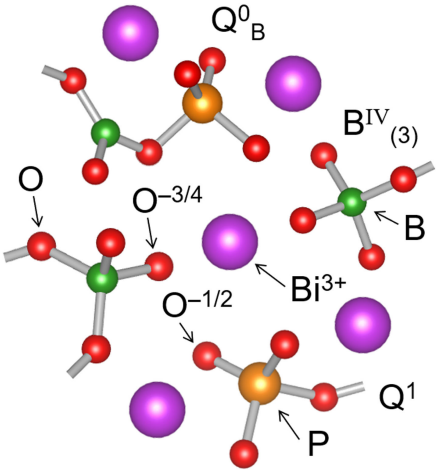

Fig. 6. The coordination structure model of a Bi^{3+} in the colorless and high refractive $50Bi_2O_3$–$20P_2O_5$–$30B_2O_3$ ($x = 50$, $y = 20$) glass, deduced from the analyses of ^{11}B and ^{31}P MAS-NMR spectroscopy.

is supportive evidence of a strong affinity for phosphate units.

Finally, it is worth noting the relationship between optical properties and coordination structure. Lone pair electrons of Bi^{3+} occupy the top of the valence band in crystalline Bi_2O_3,[19] which may compete with the O 2p electron level. Hence, the optical absorption derived from the Bi^{3+} $6s^2$–$6s^1p^1$ transition[5),19)] strongly correlates to the coordination structure around a Bi^{3+}. Therefore, the bandgap energy increase by decreasing the negative charge on the ligand oxygen. This idea agrees with the observed widened optical bandgap by substitution of P_2O_5.

4. Conclusions

The colorless, high refractive index Bi_2O_3–P_2O_5–B_2O_3 glass is realized by substation B_2O_3 by P_2O_5. The results are summarized as follows:

(1) The $50Bi_2O_3$–$20P_2O_5$–$30B_2O_3$ glass has a larger optical bandgap (~3.6 eV) and high refractive index (~2.0).

(2) The contrast in optical transmission spectra of the $50Bi_2O_3$–$20P_2O_5$–$30B_2O_3$ glass to that of the $50Bi_2O_3$–$50B_2O_3$ glass is understood because the Bi^{3+} in former glass has a solvation shell structure regulated by the phosphate anions.

(3) A weak ligand field is attributed to the less net charge belonging to NBOs of $O^{-1/2}$ or $O^{-3/4}$ around a Bi^{3+}.

(4) The Bi_2O_3–P_2O_5–B_2O_3 glasses with a wide optical bandgap, high refractive index, and small photoelastic constant are preferred to optical lenses and filters in the visible region.

5. Declaration of competing interests

The authors declare to have no interest in the present paper.

Acknowledgments This work was partially supported by JSPS KAKENHI Grant Number JP25820333. K.H. was partially supported by the JSPS Overseas Challenge Program for Young Researchers.

References

1) T. Maeder, *Int. Mater. Rev.*, 58, 3–40 (2013).
2) C. Hwang, S. Fujino and K. Morinaga, *J. Am. Ceram. Soc.*, 87, 1677–1682 (2004).
3) C. P. E. Varsamis, N. Makris, C. Valvi and E. I. Kamitsos, *Phys. Chem. Chem. Phys.*, 23, 10006–10020 (2021).
4) A. Saitoh, G. Tricot, P. Rajbhandari, S. Anan and H. Takebe, *Mater. Chem. Phys.*, 149–150, 648–656 (2015).
5) A. Saitoh, K. Hayashi, K. Hanzawa, S. Ueda, S. Kawachi, J. Yamaura, K. Ide, J. Kim, G. Tricot, S. Matsuishi, K. Mitsui, T. Shimizu, M. Mori, H. Hosono and H. Hiramatsu, *J. Non-Cryst. Solids*, 560, 12072001–12072014 (2021).
6) K. Hayashi, T. Shimizu, S. Matsuishi, H. Hiramatsu and A. Saitoh, *J. Mater. Sci.-Mater. El.*, 33, 2242–2256 (2022).
7) A. Saitoh, S. Matsuishi, M. Oto, T. Miura, M. Hirano and H. Hosono, *Phys. Rev. B*, 72, 1–4 (2005).
8) A. Saitoh, S. Matsuishi, C. Se-Weon, J. Nishii, M. Oto, M. Hirano and H. Hosono, *J. Phys. Chem. B*, 110, 7617–7620 (2006).
9) P. Roychoudhury, A. Paul, S. Mukherjee and K. Goswami, *Phys. Chem. Glasses*, 42, 126–132 (2001).
10) T. Hashimoto, Y. Shimoda, H. Nasu and A. Ishihara, *J. Am. Ceram. Soc.*, 94, 2061–2066 (2011).
11) G. Tricot, A. Saitoh and H. Takebe, *Phys. Chem. Chem. Phys.*, 17, 29531–29540 (2015).
12) D. Massiot, F. Fayon, M. Capron, I. King, S. Le Calve, B. Alonso, J. O. Durand, B. Bujoli, Z. Gan and G. Hoatson, *Magn. Reson. Chem.*, 40, 70–76 (2002).
13) M. Oto, S. Kikugawa, T. Miura, M. Hirano and H. Hosono, *J. Non-Cryst. Solids*, 349, 133–138 (2004).
14) G. A. N. Connel, in "Amorphous Semiconductors", Ed. by M. H. Brodsky, Springer-Verlag, New York (1974).
15) B. Raguenet, G. Tricot, G. Silly, M. Ribes and A. Pradel, *J. Mater. Chem.*, 21, 17693–17704 (2011).
16) T. Uchino and Y. Ogata, *J. Non-Cryst. Solids*, 181, 175–188 (1995).
17) B. Gamoke, D. Neff and J. Simons, *J. Phys. Chem. A*, 113, 5677–5684 (2009).
18) K. Mitsui, K. Suzuki and A. Saitoh, *Jpn. J. Appl. Phys.*, 61, 0955071–0955077 (2022).
19) A. Walsh, G. W. Watson, D. J. Payne, R. G. Edgell, J. Guo, P.-A. Glans, T. Learmonth and K. E. Smith, *Phys. Rev. B*, 73, 2351041–23510413 (2006).